Four-spin cross relaxation in a hybrid quantum device

Cheng Ma,[1,*] Zhiling Wang,[1,*] Yukai Wu,[1,2] Zenghui Bao,[1] Yipu Song,[1] Hongyi Zhang,[1,†] and Luming Duan[1,‡]

[1]*Center for Quantum Information, Institute for Interdisciplinary Information Sciences, Tsinghua University, Beijing 100084, People's Republic of China*

[2]*Department of Physics, University of Michigan, Ann Arbor, Michigan 48109, USA*

(Received 10 March 2019; published 16 July 2019)

Understanding the spin relaxation in superconducting quantum circuit and solid-state spin hybrid systems is of great importance especially for quantum storage purposes. We have studied the longitudinal relaxation for electron spins of substitutional nitrogen (P1) centers in a hybrid quantum device containing a diamond and a superconducting coplanar waveguide resonator. From a series of pump-probe experiments we conclude that the dominated spin relaxation mechanism is a cross-relaxation process induced by a four-spin interaction (four-spin cross relaxation) among different hyperfine split spin transitions. Some features of the four-spin process are discussed based on a set of rate equations. This work provides interesting perspectives in understanding the coherence properties of the hyperfine split spin ensembles in a hybrid quantum system.

DOI: 10.1103/PhysRevA.100.012322

I. INTRODUCTION

The physical realization of a quantum computer currently includes a few different experimental systems like superconducting circuits, trapped ions, and solid-state spins [1–3]. A lot of remarkable progresses have been made in recent years. But for each system there are still clear obstacles that have originated from their inherent limitations. Another important road map is using a hybrid architecture that comprises different physical systems with complementary functionalities [4,5]. For example, superconducting circuits have fast information-processing speed but suffer from notable decoherence. On the other hand, solid-state spins are known to have very long coherence times but are relatively hard to manipulate. With a coherent interface between the two systems, one could use superconducting circuits for information processing and spins for quantum storage [6–8].

Such a coherent interface can be realized by coupling a large ensemble of spins to a superconducting resonator. A spin ensemble is required since the coupling strength g between a single electron spin and a coplanar waveguide (CPW) resonator is on the order of 1–10 Hz, which is too small to reach the strong-coupling regime [9,10]. For an ensemble of N spins the collective coupling strength can be as large as $g_{\mathrm{ens}} = g\sqrt{N}$ [7]. When N is large enough, g_{ens} can surpass the decoherence rate of the composing systems and the strong-coupling regime can be achieved. In recent years, many kinds of electron spins, like donor atoms in silicon, nitrogen-vacancy (NV) centers, or substitutional nitrogen (P1) centers in diamond, have successfully realized strong coupling to CPW resonators [9–15]. Quantum storage of microwave photons has also been demonstrated with those hybrid devices [16–18].

Such a hybrid device also allows for the fundamental study of the composing systems. For solid-state spins, understanding and manipulating the longitudinal spin relaxation is essential in the fields of quantum information, magnetic resonance spectroscopy, and spintronics [19,20]. In superconducting resonator and solid-state spin coupled devices researchers have observed many interesting phenomenon related to the spin relaxation process. The Purcell effect in a microwave regime has been reported when placing bismuth spins in silicon in a carefully designed superconducting resonator [20]. For nitrogen-vacancy centers in diamond, a collective coherent spin relaxation process and vacuum phonon states limiting spin relaxation have also been reported [21,22].

In this work we study the electron spin relaxation process of P1 centers in diamond. We have observed a fast longitudinal spin relaxation process with a typical longitudinal relaxation time ($T1$) on the order of 1 ms. We attribute this fast relaxation to a four-spin flip-flop-based cross-relaxation process. Some characteristics of this process are also discussed.

II. EXPERIMENT

The sample is a type Ib diamond with a nominal nitrogen impurity concentration of about 200 ppm, which is pressed on top of a CPW resonator. The CPW resonator has a fundamental resonance at $\omega_c/2\pi = 4.345$ GHz with a quality factor of $Q = 400$. The sample is loaded into a dilution refrigerator equipped with a magnetic coil for microwave transmission measurements. All measurements are carried out at a base temperature of 16 mK. More information about the sample and experimental setup can be found in Appendix A. We couple the electron spin transitions of P1 centers to the CPW fundamental resonance. Each P1 center has an unpaired electron spin that has strong hypefine interaction with the nuclear spin. The Hamiltonian is given by $H = -m_0\vec{B}\cdot\vec{S} + h\vec{S}\cdot A\cdot\vec{I}$, with $\vec{S}$ being the electron spin-1/2 operator, $\vec{I}$ being the electron spin-1 operator for the nitrogen

*These authors contributed equally to this work.
†hyzhang2016@tsinghua.edu.cn
‡lmduan@tsinghua.edu.cn

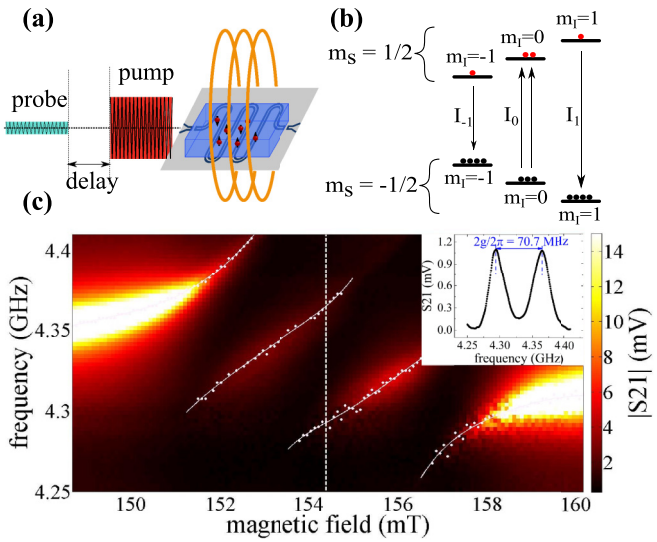

FIG. 1. (a) Illustration of the hybrid device. The magnetic field is applied along the diamond's ⟨001⟩ direction to achieve the same Zeeman splitting for all the spin transitions along the ⟨111⟩ direction. (b) Energy levels of electron spins of P1 centers considering Zeeman splitting and hyperfine splitting. (c) Intensity plot of the S_{21} spectra under varied magnetic fields. Three clear avoided crossings ambiguously manifest the strong coupling between the three electron spin transitions and the resonator mode. The white markers and lines give the fitted peak positions in each of the vertical cuts. The inset in panel (c) is a vertical cut of panel (c) at $B_\parallel = 154.4$ mT [indicated by the white dashed line in panel (c)]. It shows the vacuum Rabi split transmission peaks with a splitting value of $2g_{\rm ens}/2\pi = 70.7$ MHz.

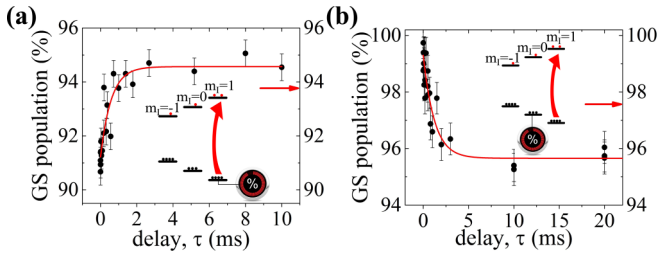

FIG. 2. (a) Fast longitudinal relaxation process for I_1 spins. Panel (a) shows the evolution of the ground-state population after pumping the I_1 spins. (b) Spin cross relaxation from $I = 1$ to $I = 0$. After pumping the I_1 spins, the GS population for I_0 spins shows a fast decay, which indicates an excitation happens to the I_0 spins after the pump pulse. The error bar gives a standard deviation of the measured data. The red (gray) arrows label the calculation results based on the four-spin model. The red (gray) line is an exponential fitting of the data points. The insets in panels (a) and (b) show illustrations of the corresponding pump-probe schemes.

nucleus, $m_0/h = 28$ MHz/mT, h is Planck's constant, and $A = \mathrm{diag}(81.33, 81.33, 114.03)$ MHz is the hyperfine interaction tensor. The direction $\hat{z}$ corresponds to the diamond's ⟨111⟩ axis. If we apply the magnetic field $B_\parallel$ along the diamond's ⟨100⟩ direction all the electron spins have the same angle as $B_\parallel$. Therefore the spins have the same hyperfine interaction, which leads to three hyperfine-split electron spin transitions separated by about 94 MHz. As shown in Fig. 1(b), they correspond to $m_I = 1, 0$ and -1, respectively. Below we label them as I_1, I_0, and I_{-1}

To characterize the coupling effect between the resonator and the electron spins of P1 centers, we measure the transmission spectra when tuning the spin transitions across the CPW resonance by sweeping $B_\parallel$. The result is shown in Fig. 1(c). Three anticrossings are observed at the resonant points of the CPW resonance and the three spin transitions. This clearly indicates that a strong coupling regime is achieved between the resonator mode and the spin transitions. As shown in the inset of Fig. 1(c), the transmission spectrum shows vacuum Rabi splitting with a split-peak distance of $2g_{\rm ens}/2\pi = 70.7$ MHz, where $g_{\rm ens}$ is the coupling strength between the spin ensemble and the resonator. It is known that $g_{\rm ens} = g\sqrt{\delta N}$, where g is the coupling strength of a single spin to the CPW resonator, and δN is the difference between the number of spins in the ground state and the excited state. The magnetic-field-induced Zeeman splitting corresponds to a temperature of about 208 mK, which means that the spins can be thermally polarized to the $m_s = -1/2$ ground state with a fidelity of more than 99%. From simulation we know that g is on the order of 10 Hz. Therefore we have the total number of spins N on the order of 1.2×10^{13}, which is consistent with the estimation based on the CPW mode volume and the density of P1 centers.

In this work we use the Rabi split peaks to monitor the ground-state (GS) population for a certain spin transition. To this end we tune $B_\parallel$ to bring the coupled system to the anticrossing point corresponding to the investigated spin transition. According to the expression of $g_{\rm ens}$, any change of the GS spin population will shift the split peaks. In the experiments we can monitor the change in the transmission intensity to deduce the peak-shift value based on adequate calibrations. The peak shift is then translated to the GS spin population. Details about this procedure can be found in Appendix A.

We use a pump-probe method to investigate the spin relaxation process. First a strong pump pulse is applied to bring some spins out of thermal equilibrium. The spins get relaxed and then weak probe tones are applied to monitor the GS population at varied pump-probe delay τ values to characterize the spin relaxation process. Figure 2(a) shows such a measurement result for the I_1 spin transition. About 9% of the spins are excited from the GS by the pump pulse. After pumping the spins relax and the GS population starts increasing to a steady-state value of about 94.5% within 3 ms. I_0 and I_{-1} spin transitions show similar relaxation behaviors. As shown in Fig. 2(a), there are still about 5.5% out-of-equilibrium spins at the steady state. They will slowly relax with a typical time constant of tens or even hundreds of seconds depending on the excitation conditions. This is commonly known as a spin diffusion process (see Appendix B).

The observed phenomenon is much faster than previously reported phonon or photon-assisted NV electron spin relaxation in diamond (see Appendix B and Ref. [19]). Different from NV spins, the large hyperfine splitting of P1 spins yields three well-distinguished transitions. The spin flip-flops among the three spin transitions may be the main contribution to the

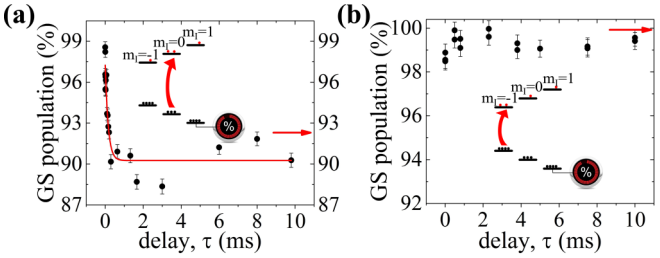

FIG. 3. The evolution of the GS population of I_1 spins after pumping at I_0 spins (a) or I_{-1} spins (b). The red (gray) arrows label the calculation results based on the four-spin model. The insets in panels (a) and (b) give illustrations of the corresponding pump-probe schemes.

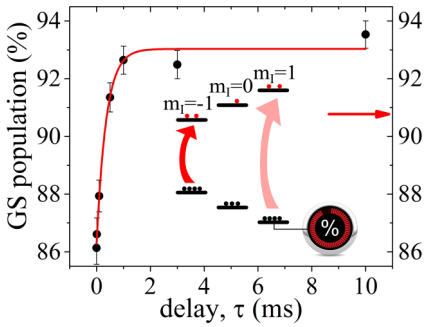

FIG. 4. Four-spin-process-mediated spin-relaxation process. A pumping pulse is firstly applied at I_1 spins. After 100 ms waiting, the system reaches a steady state and there is about 14% of spin excitation left in I_1 spins. Then we pump I_{-1} spins and probe the GS population of I_1 spins as a function of the pump-probe delay. It can be seen that the I_1 spins start relaxing to the ground state mediated by the relaxation of I_{-1} spins, which is consistent with the description of the four-spin relaxation process. The red (gray) arrows label the calculation results based on the four-spin model. The inset gives an illustration of the pump-probe scheme.

observed relaxation process via spin-spin interaction [23]. To verify this assumption we keep pumping at I_1 spins but probe I_0 spin dynamics. The result is shown in Fig. 2(b). It can be seen that more than 99% of I_0 spins stay at the ground state right after the pump pulse at I_1 spins. An interesting phenomenon happens when the I_1 pump pulse is turned off. I_0 spins are gradually excited and the GS population decreases to a steady-state value of about 96%. Compared with Fig. 2(a) it is clear that the relaxation of I_1 spins is accompanied by the excitation of I_0 spins. The two processes have similar time constants and comparable changes of the GS population. This indicates that the observed fast longitudinal spin relaxation of I_1 spins originates from a cross-relaxation process, or spin flip-flops between the two spin transitions. A similar observation has been reported by Ranjan *et al.* from a steady-state measurement [10]. They observed that saturated excitation at I_0 spins caused considerable excitation transfer to I_1 and I_{-1} transitions.

To have a better understanding of the cross-relaxation process, we turn to pump I_0 or I_{-1} spins to see how their relaxations influence I_1 spins. The result is shown in Figs. 3(a) and 3(b). It can be seen that the relaxation of I_0 spins leads to a clear excitation effect on I_1 spins, similar to the case in Fig. 2(b). On the other hand, the relaxation of I_{-1} spins has no observable excitation effect on I_1 spins. This means that the cross relaxation does not directly occur between I_1 and I_{-1} spins. It excludes the direct spin flip-flop mechanism for the cross-relaxation process. In fact, considering that the energy differences between the spin transitions are much larger than the spin linewidth (about 20 MHz), direct spin flip-flop between different spin transitions may contribute little to the cross relaxation. A high-order process, like the four-spin process that conserves the Zeeman energy, may have a greater probability to happen and become the main mechanism for spin relaxation.

As illustrated in Fig. 1(b), a four-spin flip-flop process means a flop of one I_1 spin and one I_{-1} spin accompanied by the flip of two I_0 spins [23]. Zeeman energy is conserved during such a process. It is clear that for the four-spin process the relaxation of I_1 spins would help to polarize I_{-1} spins. In order to observe such an effect we slightly modify the pump method in Fig. 3(b). Before pumping I_{-1} spins we make a prepump on I_1 spins and wait until the steady state. This introduces some excitation on I_1 spins before the following pump-probe process. As shown in Fig. 4, right after the pump pulse at I_{-1} spins, I_1 spins have a GS population of about 86% percent because of the prepump. During the relaxation of I_{-1} spins we do see a fast corelaxation of I_1 spins and the GS population of I_1 spins increases to a steady state of about 93%. This unambiguously demonstrates that the four-spin process dominates the spin relaxation.

III. DISCUSSION

We employ a theoretical model to understand the four-spin process. The four-spin process has been investigated via a quantum statistical method as shown in Ref. [24]. Here we directly present the deduced rate equation to describe such a process. Details about the derivation can be found in Appendix C and Ref. [24]. We introduce $\beta_i = \frac{1}{\hbar\omega_i}\ln\frac{N_i(-)}{N_i(+)}$, $(i = 1, 0, \text{and } -1)$ to quantify the spin excitation of the $m_I = i$ transition, where $N_i(-)$ and $N_i(+)$ represent spin numbers at the ground and excited states, respectively, and ω_i is the transition frequency for $m_I = i$ spins. The dynamics of spin relaxation can be written as

$$\frac{d\beta_0}{dt} = -W\rho, \quad \frac{d\beta_1}{dt} = \frac{\omega_0}{2\omega_1}W\rho, \quad \frac{d\beta_{-1}}{dt} = \frac{\omega_0}{2\omega_{-1}}W\rho, \tag{1}$$

where $\rho = \beta_0 - \frac{\omega_1}{2\omega_0}\beta_1 - \frac{\omega_{-1}}{2\omega_0}\beta_{-1}$, and $W = \frac{\pi}{64}N^{-3}(\frac{\sqrt{2}}{\Delta})^4 f(\frac{\mu_0\mu_B^2}{4\pi}\frac{1}{4}n\ln N)^6$ is a constant determined by the spin-spin interaction. In the expression of W, N is the total number of spins, Δ is the frequency difference between the center (I_0) and the satellite (I_1 and I_{-1}) spins, n is the density of the spins, and f is Fourier image of the spin correlation function. Details about the derivation and discussion about W can be found in Appendix C.

To get the steady-state solution we may take $\rho = 0$. Then we have

$$\begin{aligned}\beta_0 &= \left(\beta_0^0 + \frac{\omega_1}{\omega_0}\beta_1^0 + \frac{\omega_{-1}}{\omega_0}\beta_0^0\right)\Big/3,\\ \beta_1 &= \left(\frac{\omega_0}{\omega_1}\beta_0^0 + \frac{5}{2}\beta_1^0 - \frac{1}{2}\frac{\omega_{-1}}{\omega_1}\beta_{-1}^0\right)\Big/3,\\ \beta_{-1} &= \left(\frac{\omega_0}{\omega_{-1}}\beta_0^0 - \frac{1}{2}\frac{\omega_1}{\omega_{-1}}\beta_1^0 + \frac{5}{2}\beta_{-1}^0\right)\Big/3,\end{aligned} \tag{2}$$

where β_i^0 ($i = -1$, 0, and 1) is the initial value of β_i or the spin excitation of the $m_I = i$ transition at $t = 0$. We could calculate the steady-state GS population for a given initial condition with the above equations. As for our experiments, we take the $\tau \sim 0$ data based on the measured GS population as the initial conditions. For the spin transitions that are not directly pumped, the initial GS populations range from 98% to 99%, which are slightly smaller than the thermal equilibrium value due to the nonresonant excitation effect. The calculation results are presented in Figs. 2, 3, and 4 with red (gray) arrows.

It can be seen that the calculation results are in line with the measured steady-state GS populations. In other words, the four-spin model can correctly predict the excitation redistribution with a given initial spin excitation. The deviations between the experimental and the calculated results could be understood considering that the initial GS populations we used in the calculation are slightly different than the real situations. We may underestimate the initial spin excitation because of two reasons. On the one hand, the pump pulses in the experiments are relatively long compared with the relaxation dynamics. The real initial GS population could be smaller than the $\tau \sim 0$ data. On the other hand, the nonresonant pump effect is not taken into account.

An interesting phenomenon related to the four-spin process is the accelerated relaxation of I_1 spins by applying a pump at I_{-1} spins and vice versa, as shown in Fig. 4. The four-spin cross relaxation is essentially the excitation redistribution among different spin transitions. But if we are only concerned about I_1 spins, other spin transitions can be viewed as ancillas. The phenomenon mentioned above can be considered as an ancilla-assisted spin cooling effect, which can be used for an efficient spin reset. This could be helpful considering the fact that the time used for spin relaxation can be up to tens of minutes, especially at cryogenic temperatures.

Next we briefly discuss the dynamics of the four-spin process. Equation (2) can be reorganized as

$$\frac{d}{dt}(-\beta_0 + \beta_{-1}/2 + \beta_1/2) = -\frac{3}{2}W(-\beta_0 + \beta_{-1}/2 + \beta_1/2). \tag{3}$$

From the above equation one can see that the time constant for a four-spin process is proportional to $1/W$. More specifically, based on the expression of W the dynamic of four-spin cross relaxation is mainly determined by the total number of spins N, the spin density n, and the energy difference between different transitions Δ. The initial spin excitation influences the cross relaxation dynamic via the Fourier image of the correlation function f. The exact value of f is difficult to calculate. From our experimental results f is estimated to be on the order of 1 ms. The abovementioned theoretical model and discussion can be immediately used in other spin systems and hybrid quantum devices [25].

The dynamics of the observed four-spin relaxation could have a crucial impact on other spins in diamond, e.g., electron spins of NV centers, especially considering the emerging applications of quantum sensing which prefers using a large ensemble of NV centers with a considerable amount of P1 centers [26]. It has been reported that the dynamic of the spin bath is an important source of NV electron spin decoherence [27]. The four-spin cross relaxation reported here may strongly complicate the dynamic of the spin bath, which may reduce the coherence of NV spins. Therefore it is important to suppress the cross-relaxation process to have better coherence of NV spins.

IV. CONCLUSION

In conclusion, a fast longitudinal relaxation of P1 electron spins with a time constant on the order of 1 ms is observed in a diamond-CPW resonator hybrid quantum device. The fast relaxation is accompanied by an excitation or relaxation of other spin transitions. This phenomenon is understood in the frame of a four-spin cross-relaxation process. A set of rate equations is applied to describe the four-spin process, which successfully reproduces the experimental data. The dynamic of the four-spin process and its possible influence on the coherence properties of NV electron spins in diamond are also discussed. We propose that for some circumstances the four-spin process can be used for efficient spin reset.

ACKNOWLEDGMENTS

This work was supported by the Ministry of Education, the National Key Research and Development Program of China, and the National Natural Science Foundation of China under Grant No. 11874235.

APPENDIX A: SAMPLE, MEASUREMENTS, AND DATA PROCESSING

The $\lambda/2$ coplanar waveguide (CPW) resonator was patterned in 100-nm-thick sputtered niobium film on a 500-μm-thick high-resist silicon substrate. The resonator has a fundamental resonance at $\omega_c/2\pi = 4.345$ GHz with a quality factor of $Q = 400$. The diamond sample is a commercially available type Ib high-temperature high-pressure diamond with a polished (100) surface. It is specified to contain a nitrogen impurity concentration of about 200 ppm. Before the diamond was pressed onto the resonator, the diamond was processed with the oxygen-based inductively coupled plasma (ICP) to remove the surface conductive layer, which may act as a loss channel for the resonator. We found that after removing the surface conductive layer the internal quality factor Q_i of the CPW resonator had risen from 1500 to about 59 000.

The sample was loaded into a dilution refrigerator equipped with a magnetic coil and cooled down to a base temperature of about 16 mK. We applied a magnetic field of about 150 mT along the diamond's ⟨100⟩ direction to bring the

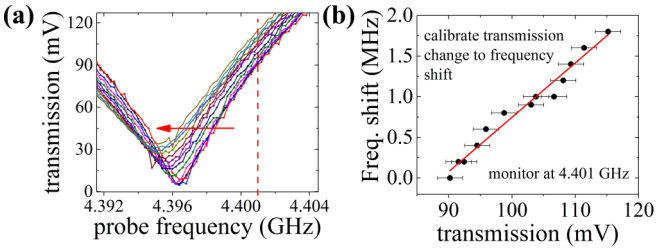

FIG. 5. Calibration of the measured transmission intensity to the frequency shift of the VRS. Panel (a) shows one of the VRS peaks at different pump powers. The pump tone diminished the ground-state spin population and the VRS peaks shift correspondingly. As shown in panel (b), for a given frequency of $f = 4.401$ GHz [indicated by a red dashed line in panel (a)] we could calibrate the strength of the transmission signal to the frequency shift. The error bars give standard deviations of the measured data points.

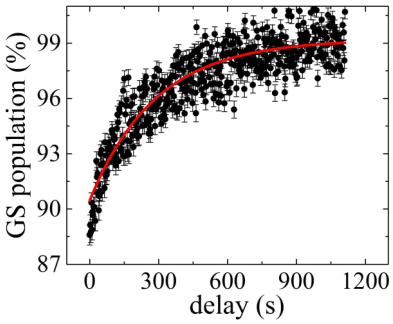

FIG. 6. The slow spin diffusion process. The residual spin excitation after the four-spin relaxation process will be slowly relaxed with a time constant of about hundreds of seconds. Such a process is commonly known as spin diffusion out of the resonator mode region. The error bars give the standard deviations of the data points.

spin transitions on resonance to the $\lambda/2$ mode of the resonator. The magnetic-field-induced Zeeman splitting corresponds to a temperature of about 208 mK. This means that the spins can be thermally polarized to the $m_s = 1/2$ ground state with a fidelity of more than 99%. The time resolved transmission spectra of the device were measured with a homodyne method. The square pulses for pump or probe purposes were generated by the gated outputs from microwave generators. The typical length of the pump and probe pulses was 500 μs. Then they were attenuated by 50 dB in the fridge and sent to the sample. A fast microwave switch was used to send only the probe pulses to the amplifiers to prevent any possible overload or even damage to the amplifiers by the strong pump pulses. After amplifications, the probe signal was mixed down to DCdc with an IQ mixer and recorded by a fast analog to digital converter with a 1 GHz sampling rate. More than 40 min of waiting time was used between the adjacent trails to guarantee a complete spin relaxation.

We used a calibration method to map the measured transmission intensity to the ground state (GS) population for a given spin transition. In the strong-coupling regime, when the spin transition frequency is aligned to the resonator frequency, the transmission spectra of the coupled system is characterized by vacuum Rabi splitting (VRS), as shown in the inset of Fig. 1(c). The splitting value $g_{\rm ens} = g\sqrt{\delta N}$ is determined by the difference between the number of spins in the ground state and the excited state δN. A small change of δN that keeps the system in the strong-coupling regime will shift the VRS peaks. Therefore we can tell the GS spin population by measuring the VRS peak shift. As shown in Fig. 5, the VRS peak shift can be measured by monitoring the change of transmission intensity at a certain frequency around the split peaks. With such a calibration process, we can get the GS spin population by measuring the transmission intensity at a certain frequency.

APPENDIX B: SPIN DIFFUSION AND THE PURCELL EFFECT

The spatial inhomogeneity of the electromagnetic field is an intrinsic character of CPW structures. As a consequence, spin excitation through the CPW structures also suffers from spatial inhomogeneity. Such an inhomogeneous excitation will get relaxed via the spin diffusion process. In Figs. 2 to 4, we find that for steady states of the four-spin cross-relaxation processes there is still a part of spins not relaxed to the ground state. The relaxation for this part of spins will mainly take the form of spin diffusion with a time constant ranging from tens of seconds to hundreds of seconds. An example of the spin-diffusion-assisted relaxation can be found in Fig. 6.

We would like to argue that the Purcell effect could be negligible in our case. We could make a simple estimation based on the Purcell-effect-dominated spontaneous emission rate $\Gamma = \kappa \frac{g^2}{\kappa^2/4+\delta^2}$, where κ is the resonator damping rate, g is the single spin-resonator coupling strength, and δ is the spin-resonator detuning. The resonator used in the experiment has a loaded Q value of about 400; therefore $\kappa/2\pi = f/Q$ is on the order of 10 MHz, where f is the resonator frequency. As mentioned previously, g is on the order of 10 Hz. When the spins and the resonator are on resonance the estimated Purcell rate is on the order of 10^{-4} Hz, which is much slower than the time scale covered in the main text.

APPENDIX C: THEORETICAL DESCRIPTION OF THE FOUR-SPIN PROCESS

The Hamiltonian of the P1 electron spins can be written as [24]

$$
\begin{aligned}
H &= H_0 + H_{0i} + H_i, \quad H_0 = \sum_n \omega_n \sum_i S^z_{ni}, \\
H_{0i} &= \frac{1}{2}\sum_{ij,n,n'} v^{zz}_{ij} S^z_{ni} S^z_{n'j} + \sum_{ij,n} v^{\pm}_{ij} S^+_{ni} S^-_{nj}, \\
H_i &= \frac{1}{2}\sum_{ij} v^{\pm}_{ij} (S^+_{1i} S^-_{0j} + S^-_{1i} S^+_{0j}) \\
&\quad + \frac{1}{2}\sum_{ik} v^{\pm}_{ik} (S^+_{1i} S^-_{-1k} + S^-_{1i} S^+_{-1k}) \\
&\quad + \frac{1}{2}\sum_{jk} v^{\pm}_{ij} (S^+_{-1k} S^-_{0j} + S^-_{-1k} S^+_{0j}).
\end{aligned} \tag{C1}
$$

Here H_0 is the Zeeman energy of the spin ensemble, H_{0i} represents the z-z coupling among spins in the subsystem $m_I = i$, and spin flip-flop in any subsystem fulfills the energy conservation. The last term H_i indicates a possible flip-flop process between subsystems. $S^z_{ni}(S^\pm_{ni})$ represents the z operator (ladder operator) of the ith spin in subsystems $n = -1, 0$, and 1. $v^{zz}_{ij}(v^\pm_{ij})$ represents the strength of dipole-dipole interaction between two spins i and j in different components.

In order to meet the requirement of energy conservation, this kind of process shall include at least four spins: one spin in $m_I = -1$, one in $m_I = 1$, and two spins in $m_I = 0$. Other possible processes shall contain more spins in order to fulfill energy conservation, which will be a higher-order process and have lower rates.

With the method of the nonequilibrium statistical operator of Zubarev [24,28], we can get the rate equations in the main text by using two conditions. First, the energy differences between the hyperfine split structures of P1 centers are about 95 MHz, or a characteristic temperature of about $T_c = 5$ mK. The base temperature of our fridge is about 16 mK $\gg T_c$, which would not lead to an obvious initial nuclear spin polarization; therefore we can take $N_{-1} = N_1 = N_0$. Second, we suppose $\omega_{-1} + \omega_1 = 2\omega_0$; if this condition is not satisfied, lattice temperature has to be taken into consideration to guarantee the conservation of the energy. Details about the derivation can be found in Ref. [24].

As discussed in the main text, the dynamic of the four-spin flip-flop process is mainly determined by W. From the abovementioned derivation, W is defined as

$$W = \frac{\pi}{64}\frac{1}{N_1}\sum_{i,i',j,k}^{N_0N_0N_1N_{-1}}\left|\frac{v^\pm_{ij}v^\pm_{i'j}}{\omega_0-\omega_1}+\frac{v^\pm_{ik}v^\pm_{i'k}}{\omega_0-\omega_{-1}}\right|^2 \times\left|\frac{v^\pm_{jk}}{\omega_{-1}-\omega_1}\right|^2[F_1(\delta)+F_2(\delta)]. \tag{C2}$$

Here $F_1(\delta)$ and $F_2(\delta)$ are Fourier images of two spin correlation functions,

$$f_1(t) = \frac{\langle S^-_{0i}S^-_{0i'}S^+_{1j}S^+_{-1k}S^+_{0i}(t)S^+_{0i'}(t)S^-_{1j}(t)S^-_{-1k}(t)\rangle}{\langle S^-_{0i}S^-_{0i'}S^+_{1j}S^+_{-1k}S^+_{0i}S^+_{0i'}S^-_{1j}S^-_{-1k}\rangle},$$
$$f_2(t) = \frac{\langle S^+_{0i}S^+_{0i'}S^-_{1j}S^-_{-1k}S^-_{0i}(t)S^-_{0i'}(t)S^+_{1j}(t)S^+_{-1k}(t)\rangle}{\langle S^+_{0i}S^+_{0i'}S^-_{1j}S^-_{-1k}S^-_{0i}S^-_{0i'}S^+_{1j}S^+_{-1k}\rangle}, \tag{C3}$$

and $\delta = \omega_{-1} + \omega_1 - 2\omega_0$ is the energy change of a four-spin flip-flop event. In our case here $\delta = 0$. We take some approximation to simplify the expression of W. It is reasonable to use the averaged interaction strength among spins in different subsystems, we can take $v = v^\pm_{ij} = v^\pm_{i'j} = v^\pm_{jk} = v^\pm_{ik} = v^\pm_{i'k}$. To rewrite the expression of W we take $f = [F_1(\delta) + F_2(\delta)]$ and $\Delta = \omega_1 - \omega_0 = \omega_0 - \omega_{-1}$; therefore we have

$$W = \frac{\pi}{64}N^3\left(\frac{2}{\Delta}\right)^2\left(\frac{1}{\Delta}\right)^2 f v^6. \tag{C4}$$

In previous discussion, we have neglected the inhomogeneous broadening of the spin linewidth. Here we make a simple discussion on the influence of the inhomogeneity and argue that it has a minor effect on our theoretical model. As mentioned in the main text we use the constant W to represent the rate of the spin cross relaxation. From Eq. (C4) we know that W is proportional to the energy difference Δ to the power of -4. Suppose the inhomogeneously broadened spin profile has a Gaussian distribution of $P(E_i|E_i^0,\sigma) = \frac{1}{\sqrt{2\pi\sigma^2}}\exp^{-\frac{(E_i-E_i^0)^2}{2\sigma^2}}$, where σ is the spin linewidth, and E_i^0 is the center frequency of $m_I = -1$, 0, and 1 spins. Then in the expression of W we have $\langle\frac{1}{\Delta^4}\rangle = \int_{E_i-4\sigma}^{E_i+4\sigma}dE_i\int_{E_j-4\sigma}^{E_j+4\sigma}dE_jP(E_i)P(E_j)(E_i-E_j)^{-4}$. There is a cutoff for the reciprocal integration. In our experiment the spin linewidth is about 20 MHz. It yields $\sigma = 20/2.335 = 8.6$ MHz, leading to a result of $\langle\frac{1}{\Delta^4}\rangle = 1.47\times10^{-8}$. When not considering the inhomogeneous broadening, we have the mean energy difference $\Delta = 95$ MHz, leading to $\frac{1}{\Delta^4} = 1.22\times10^{-8}$. Comparing the value of $\langle\frac{1}{\Delta^4}\rangle$ and $\frac{1}{\Delta^4}$, we know that the spin diffusion process should be faster considering the inhomogeneous broadening. Also because of the minor difference between these two results, we can safely neglect the inhomogeneity of the spin profile in the following discussion for simplicity.

We could further derive the expression of v. Considering two spins separated with a distance r and an angle θ, the interaction strength v can be written as

$$v = \frac{\mu_0\mu_B^2}{4\pi}\frac{1}{4}\frac{1}{r^3}(1-3\cos^2\theta). \tag{C5}$$

For simplification we abort the polar angle θ but, using an average spin-spin distance, then we have

$$v = \frac{\mu_0\mu_B^2}{4\pi}\frac{1}{4}\left\langle\frac{1}{r^3}\right\rangle. \tag{C6}$$

Considering the three-dimensional distribution of the spins, $\langle\frac{1}{r^3}\rangle$ can be written as

$$\left\langle\frac{1}{r^3}\right\rangle = \frac{1}{N}\sum\frac{1}{r} = \int_{r_0}^{R}\frac{N}{4\pi R^3/3}4\pi r^2dr\frac{1}{r^3} = \frac{3}{R^3}\int_{r_0}^{R}\frac{dr}{r} = \frac{3}{R^3}\ln\frac{R}{R/N^{1/3}} = \frac{1}{R^3}\ln N = \frac{\ln N}{N/n}, \tag{C7}$$

where N is total number of spins and n is the spin density. Therefore we could write W as $W = \frac{\pi}{64}N^{-3}(\frac{\sqrt{2}}{\Delta})^4 f(\frac{\mu_0\mu_B^2}{4\pi}\frac{1}{4}n\ln N)^6$, which is the expression in the main text.

Equations (1) in the main text are in the form of a first-order ordinary differential equation $\dot{x}(t) = Ax(t)$, where the matrix A has two eigenvalues equal to 0 and one nonzero eigenvalue. This implies that there should be two invariants and one dynamical process. By taking $\rho = 0$, the steady-state result can be obtained.

[1] C. Neill *et al.*, Science **360**, 195 (2018).

[2] C. Monroe and J. Kim, Science **339**, 1164 (2013).

[3] D. D. Awschalom, L. C. Bassett, A. S. Dzurak, E. L. Hu, and J. R. Petta, Science **339**, 1174 (2013).

[4] G. Kurizki, P. Bertet, Y. Kubo, K. Molmer, D. Petrosyan, P. Rabl, and J. Schmiedmayer, Proc. Natl. Acad. Sci. USA **112**, 3866 (2015).

[5] J. H. Wesenberg, A. Ardavan, G. A. D. Briggs, J. J. L. Morton, R. J. Schoelkopf, D. I. Schuster, and K. Molmer, Phys. Rev. Lett. **103**, 070502 (2009).

[6] B. Julsgaard, C. Grezes, P. Bertet, and K. Molmer, Phys. Rev. Lett. **110**, 250503 (2013).

[7] A. Imamoğlu, Phys. Rev. Lett. **102**, 083602 (2009).

[8] I. Diniz, S. Portolan, R. Ferreira, J. M. Gérard, P. Bertet, and A. Auffèves, Phys. Rev. A **84**, 063810 (2011).

[9] R. Amsuss, C. Koller, T. Nobauer, S. Putz, S. Rotter, K. Sandner, S. Schneider, M. Schrambock, G. Steinhauser, H. Ritsch, J. Schmiedmayer, and J. Majer, Phys. Rev. Lett. **107**, 060502 (2011).

[10] V. Ranjan, G. de Lange, R. Schutjens, T. Debelhoir, J. P. Groen, D. Szombati, D. J. Thoen, T. M. Klapwijk, R. Hanson, and L. DiCarlo, Phys. Rev. Lett. **110**, 067004 (2013).

[11] X. Zhu, S. Saito, A. Kemp, K. Kakuyanagi, S. Karimoto, H. Nakano, W. J. Munro, Y. Tokura, M. S. Everitt, K. Nemoto, M. Kasu, N. Mizuochi, and K. Semba, Nature (London) **478**, 221 (2011).

[12] D. L. Creedon, J.-M. Le Floch, M. Goryachev, W. G. Farr, S. Castelletto, and M. E. Tobar, Phys. Rev. B **91**, 140408(R) (2015).

[13] B. C. Rose, A. M. Tyryshkin, H. Riemann, N. V. Abrosimov, P. Becker, H. J. Pohl, M. L. W. Thewalt, K. M. Itoh, and S. A. Lyon, Phys. Rev. X **7**, 031002 (2017).

[14] D. I. Schuster, A. P. Sears, E. Ginossar, L. DiCarlo, L. Frunzio, J. J. L. Morton, H. Wu, G. A. D. Briggs, B. B. Buckley, D. D. Awschalom, and R. J. Schoelkopf, Phys. Rev. Lett. **105**, 140501 (2010).

[15] Y. Kubo, F. R. Ong, P. Bertet, D. Vion, V. Jacques, D. Zheng, A. Dréau, J. F. Roch, A. Auffeves, F. Jelezko, J. Wrachtrup, M. F. Barthe, P. Bergonzo, and D. Esteve, Phys. Rev. Lett. **105**, 140502 (2010).

[16] C. Grezes, B. Julsgaard, Y. Kubo, W. L. Ma, M. Stern, A. Bienfait, K. Nakamura, J. Isoya, S. Onoda, T. Ohshima, V. Jacques, D. Vion, D. Esteve, R. B. Liu, K. Mølmer, and P. Bertet, Phys. Rev. A **92**, 020301(R) (2015).

[17] C. Grezes, B. Julsgaard, Y. Kubo, M. Stern, T. Umeda, J. Isoya, H. Sumiya, H. Abe, S. Onoda, T. Ohshima, V. Jacques, J. Esteve, D. Vion, D. Esteve, K. Mølmer, and P. Bertet, Phys. Rev. X **4**, 021049 (2014).

[18] Y. Kubo, C. Grezes, A. Dewes, T. Umeda, J. Isoya, H. Sumiya, N. Morishita, H. Abe, S. Onoda, T. Ohshima, V. Jacques, A. Dréau, J. F. Roch, I. Diniz, A. Auffeves, D. Vion, D. Esteve, and P. Bertet, Phys. Rev. Lett. **107**, 220501 (2011).

[19] A. Jarmola, V. M. Acosta, K. Jensen, S. Chemerisov, and D. Budker, Phys. Rev. Lett. **108**, 197601 (2012).

[20] A. Bienfait, J. J. Pla, Y. Kubo, X. Zhou, M. Stern, C. C. Lo, C. D. Weis, T. Schenkel, D. Vion, D. Esteve, J. J. L. Morton, and P. Bertet, Nature (London) **531**, 74 (2016).

[21] A. Angerer, K. Streltsov, T. Astner, S. Putz, H. Sumiya, S. Onoda, J. Isoya, W. J. Munro, K. Nemoto, J. Schmiedmayer, and J. Majer, Nat. Phys. **14**, 1168 (2018).

[22] T. Astner, J. Gugler, A. Angerer, S. Wald, S. Putz, N. J. Mauser, M. Trupke, H. Sumiya, S. Onoda, J. Isoya, J. Schmiedmayer, P. Mohn, and J. Majer, Nat. Mater. **17**, 313 (2018).

[23] P. P. Sorokin, G. J. Lasher, and I. L. Gelles, Phys. Rev. **118**, 939 (1960).

[24] C. K. Mai, Phys. Status Solidi B **66**, 433 (1974).

[25] X. Zhang, C. L. Zou, N. Zhu, F. Marquardt, L. Jiang, and H. X. Tang, Nat. Commun. **6**, 8914 (2015).

[26] N. Bar-Gill, L. M. Pham, C. Belthangady, D. Le Sage, P. Cappellaro, J. R. Maze, M. D. Lukin, A. Yacoby, and R. Walsworth, Nat. Commun. **3**, 858 (2012).

[27] J. Xing, Y.-C. Chang, N. Wang, G.-Q. Liu, and X.-Y. Pan, Chin. Phys. Lett. **33**, 107601 (2016).

[28] D. N. Zubarev, *Nonequilibrium Statistical Thermodynamics* (Consultants Bureau, New York, USA, 1974).